PCCP

Gas-Phase Pyrolysis of *trans* 3-Pentenenitrile: Competition between Direct and Isomerization-Mediated Dissociation

Journal:	*Physical Chemistry Chemical Physics*
Manuscript ID	CP-ART-01-2021-000104
Article Type:	Paper
Date Submitted by the Author:	09-Jan-2021
Complete List of Authors:	Mishra, Piyush; Purdue University, Department of Chemistry; Massachusetts Institute of Technology, Department of Chemistry Fritz, Sean; Purdue University, Department of Chemistry; Vertex Pharmaceuticals Inc Herbers, Sven; Purdue University, Department of Chemistry; Universität zu Köln, Institute of Physics Mebel, Alexander; Florida International University, Chemistry and Biochemistry Zwier, Timothy; Purdue University, Department of Chemistry; Sandia National Laboratories California, Combustion Research Facility

Gas-Phase Pyrolysis of *trans* 3-Pentenenitrile: Competition between Direct and Isomerization-Mediated Dissociation

Piyush Mishra[1,a], Sean M. Fritz[1,b], Sven Herbers[1,c], Alexander M. Mebel[2]* and Timothy S. Zwier[1,3]*

[1]*Department of Chemistry, Purdue University, West Lafayette, IN 47907-1393 U.S.A*

[2]*Department of Chemistry, Florida International University, Miami, FL 33199 U.S.A.*

[3]*Combustion Research Facility, Sandia National Laboratories, Livermore, CA 94550 U.S.A.*

Abstract

The flash pyrolysis of *trans* 3-pentenenitrile (3-PN, CH_3-CH=CH-CH_2-CN) was studied by combining the results of VUV photoionization mass spectra with broadband microwave spectra recorded as a function of the temperature of the pyrolysis tube. The two separated functional groups (vinyl and nitrile) open up isomerization as an initial step in competition with unimolecular dissociation. Primary products were detected by keeping the 3-PN concentration low and limiting reaction times to the traversal time of the gas in the pyrolysis tube (~100 μs). The reaction is quenched and products are cooled by expansion into vacuum before interrogation over the 8-18 GHz region using chirped-pulse broadband methods. 118 nm VUV photoionization of the same reaction mixture provides a means of detecting all products with ionization potentials below 10.5 eV with minimal fragmentation. These results are combined with a detailed computational investigation of the C_5H_7N and related potential energy surfaces, leading to a consistent picture of the unimolecular decomposition of 3-PN. Loss of two H-atoms to form a 79 amu product is proven from its microwave transitions to contain *trans*-Z-2,4-pentadienenitrile, while no pyridine is observed. Methyl loss, HCN loss, and breaking the central C(2)-C(3) bond all occur following isomerization of the position of the double bond, thereby opening up low-energy pathways to these decomposition channels.

[a]Current Address: Department of Chemistry, Massachusetts Institute of Technology, Cambridge, MA- 02139.
[b]Current address: Vertex Pharmaceuticals, Boston, MA-02210
[c]Current address: Institute of Physics I, Universität zu Köln, Zülpicher Straße 77, 50937 Köln

I. Introduction

Nitriles are found in the interstellar medium and circumstellar shells. According to a review by McGuire in late 2018,[1] nitriles comprise about 18% of the compounds detected in space, including long-chain nitrile-capped poly-ynes, and most recently, c-C_6H_5CN, the aromatic benzonitrile.[2] Due to their large permanent dipole moments and characteristic ^{14}N (I=1) nuclear quadrupole hyperfine splitting (hfs), interrogating the structure of nitrile-containing compounds with microwave and millimeter wave spectroscopy is an ideal choice. Nitriles are also important in the planetary atmospheres of our solar system, most noticeably in Titan's atmosphere, which is predominantly reducing (~3% CH_4, trace O_2) with abundant N_2 (>95%).[3] The chemical composition of Titan's atmosphere is dominated by solar-driven photochemistry, with vacuum ultraviolet (VUV) photons breaking up N_2 in the upper atmosphere and the N atoms getting incorporated into the hydrocarbons, primarily as nitriles.[3] At lower altitudes, the organic compounds build in concentration and condense, producing a layered haze that envelops the moon's surface. After the remarkable success of the Cassini-Huygens mission to interrogate the atmospheric chemical composition of Titan, the recently-approved Dragonfly drone mission is expected to provide a similarly detailed characterization of Titan's surface chemistry. The surface is thus likely to contain a rich mixture of larger nitrogen-containing organic molecules.

Pentenenitriles (C_5H_7N, PNs) have not yet been detected in extraterrestrial media, but their existence can be anticipated via radical recombination reactions. A probable formation route to 4-pentenenitrile (4-PN, CH_2=CH-CH_2-CH_2-C≡N) is via recombination of resonance stabilized cyanomethyl ($\dot{C}H_2$-CN) and allyl ($\dot{C}H_2$-CH=CH_2) radicals, due to the build-up of these unusually stable species. The isomerization of 4-pentenenitrile to 3-pentenenitrile (CH_2-CH=CH_2-CH_2-CN) is exothermic, arising from the energetic preference of secondary alkenes over primary alkenes.[4] PNs have also been detected by gas chromatography of laboratory-based Titan tholins produced by processing methane/N_2 mixtures.[5,6]

The PNs are also worthy of attention as potential intermediates along the pathway to heteroaromatics such as pyridine (C_5H_5N). Absorption in the deep UV could provide the energy needed to dissociate PNs by loss of 2H or H_2, rearrange its π-bonds, and hence its structure, to form conjugated molecules like 2,4-pentadienenitrile (CH_2=CH-CH=CH-CN, 2,4-PDN), either in a single step or in sequence. Pentadienenitriles (PDNs) are likely present in star-forming regions, and thus have garnered attention.[7–12] Especially in chemically rich regions of outer space where the chemistry is heavily dependent on radiation, one anticipates the formation of such compounds.

Pyridine is isomeric to the PDNs, and as the prototypical nitrogen heteroaromatic, establishing reaction pathways to its formation would constitute an important step towards understanding the steps along the pathway to nitrogen heteroaromatics present in the nucleic acids, that are among the fundamental building blocks of life.[13] Experimental and theoretical work has found stationary points on the C_5H_5N potential energy surface (PES) joining the PDNs, including 2,4-PDN, to pyridine.[14] The foundation for the present research lies in our previous work that structurally characterized all the conformers of 3-pentenenitrile and 4-pentenenitrile using broadband microwave spectroscopy (8-18 GHz), including the fitting of ^{14}N hyperfine splittings of both molecules and methyl internal rotation of 3-pentenenitrile.[4] Similar millimeter wave (mmW) spectroscopy of laboratory synthesized PDN isomers has been carried out by the Wisconsin group.[12,15]

Chirped-Pulse Fourier Transform Microwave (CP-FTMW) spectroscopy, pioneered by Pate and co-workers, is a powerful tool to determine high-precision microwave transition frequencies of gas-phase molecules and from them, derive their structures.[16] By combining frequency chirps with fast digitization of the molecular free-induction decay, the data acquisition process is about 1000 times faster than in cavity-based methods.[16,17] In the present work, broadband spectra cover the 8-18 GHz range. The patterns of transitions present in the spectrum provide high-precision structural information via the rotational constants and dipole moment projections along the three inertial axes. Since the introduction of this technique, its applications have grown rapidly.[18–22]

Although CP-FTMW is well suited to study multi-component samples, monitoring chemical reactions can be quite challenging, even when utilizing the predictions from calculations to guide the assignment process. This is especially the case when the reactions of interest have not been studied or characterized before. Furthermore, products or reactive intermediates that are non-polar or weakly polar ($\mu < 1$ Debye) are not easily detected since the broadband microwave signal intensity scales as μ^2.[23] In addition, detection sensitivity is maximized by cooling to low temperatures, which can be challenging when flash pyrolysis from a hot source is of interest. Hence, it is beneficial to employ a complementary analytical tool such as a mass spectrometer in tandem with the microwave spectrometer. Apart from online monitoring of the conditions and stability of the post-pyrolytic expansion, the mass-resolved detection of components with small or absent dipole moments reduces the number of possible structures that need to be analyzed in the broadband rotational spectrum.

In this work, we use our mass-correlated CP-FTMW spectrometer,[24] to perform VUV photoionization time-of-flight (TOF) mass spectrometry while acquiring our broadband microwave spectra, adding an extra dimension to our analytical capabilities. The advantage of using a vacuum ultraviolet (VUV) photoionization source (118 nm), is that it is a soft ionization technique via a single photon ionization process, thereby minimizing fragmentation of the expansion components upon photoionization. As we shall see, the two methods nicely complement each other, and both are essential to obtain a deeper understanding of the pyrolysis reactions.

There are multiple ways to initiate radical reactions of PNs, including using a discharge source, laser photolysis or flash pyrolysis. In the present study, we have carried out flash pyrolysis of *trans*-3-pentenenitrile (hereafter 3-PN), studying its thermal degradation over the 290-1100 K temperature range using a combination of CP-FTMW spectroscopy and VUV photoionization-TOF mass spectrometry.[24] We have identified both free radical and molecular reaction intermediates. As we shall see, the VUV photoionization mass spectra recorded over a range of pyrolysis source temperatures, show several peaks that grow in and decay as a function of pyrolysis nozzle temperature. Among them, appears a peak at 79 Da associated with a pyrolysis intermediate with molecular formula C_5H_5N. While pyridine was not positively identified in the microwave spectrum, we have identified transitions ascribable to s-*trans*-Z-2,4-pentadienenitrile (tZ-2,4-PDN) within the broadband rotational spectrum, and have calculated several reaction pathways to formation of chemical species observed in the microwave and mass spectra.

II. Methods

A. Experimental

The mass-correlated CP-FTMW spectrometer is elaborated elsewhere;[24] hence, we describe it only briefly here. Spectroscopy was performed on analytes supersonically cooled to rotational temperatures of T_{rot} <5K, post-pyrolysis. 3-PN (Signa Aldrich, 95%), predominantly as the *trans* isomer, was used without further purification. The sample was placed in a sample holder immediately before the pulsed valve with no direct heating of the sample. With argon backing gas in the 1.4-3.3 bar range, 3-PN was present at an estimated concentration of 0.3% in the pyrolysis tube. A pulsed valve operating at 10 Hz with a 1 mm diameter orifice was used to inject gas pulses into the pyrolysis tube (Parker General Valve Series 9). The chamber incorporates a TOF mass spectrometer that is located after the microwave interrogation zone of our CP-FTMW chamber for fast simultaneous measurement. Our instrument has three parts: (1) The pulsed valve/pyrolysis microreactor, (2) the microwave spectrometer, and (3) the mass spectrometry chamber. The source and TOF chambers are differentially pumped, separated by a skimmer of 2 mm diameter.

Flash Pyrolysis Microreactor: To perform pyrolysis experiments, a flash pyrolysis microreactor was utilized,[25] which is a modified version of the Chen nozzle.[26] This pyrolysis source has been used in previous work for spectroscopic interrogation of reactive intermediates.[18,19,22,25,27–31] The SiC pyrolysis tube

is affixed as an extension of the pulsed valve. The SiC tube (Saint-Gobain Ceramics, Hexoloy SE, 2mm dia. X 3.5 cm long) can be resistively heated to temperatures up to 1900 K. A copper heat sink cooled by chilled water protects the temperature-sensitive components of the pulsed valve and enables better independent control of sample and reactor temperatures. The temperature of the SiC tube wall is monitored by a W/Re type C thermocouple. Resistive heating is achieved by use of a variable voltage source (Variac) and a simple circuit consisting of six 250-watt light bulbs connected in parallel with one another as ballast resistor, connected in series with the SiC tube.

Vacuum Chamber: The spectroscopic chamber is evacuated by two 25 cm diameter diffusion pumps (Varian VHS 10) backed by a roots blower, with an operating pressure in the spectroscopic chamber of $\sim 1\times10^{-4}$ mbar with a gas load of 0.85 bar·cm^3/s. The interior of the microwave portion of the chamber is covered with microwave absorber material (Emerson and Cuming Eccosorb HR-25/ML; LS-24) to minimize microwave reflections from the walls of the chamber. The time-of-flight (TOF) mass spectrometer consists of a Wiley-McLaren ion source with a 1 m TOF tube, which is evacuated by a turbomolecular pump (Osaka Vacuum TG350F) backed by a roughing pump, with an operating pressure of $\sim 5\times10^{-7}$ mbar.[24]

Microwave Spectrometer: The microwave spectrometer is composed of fast electronic circuits for creation and detection of microwaves over the 2-18 GHz region. In the current work we focused attention on the 8-18 GHz region. An arbitrary waveform generator (Tektronix AWG7101, 10 GSa/s) is used to generate broadband chirps and timing markers that are used to trigger the microwave electronic components. Output frequencies from the AWG (0 to 5 GHz) are up-converted and amplified by a 200 W traveling wave-tube amplifier (TWTA; Amplifier Research 200T8G18A), which is then broadcast into the vacuum chamber through a microwave horn. The center of the microwave horns is located about 12.5 cm from the nozzle orifice. The pyrolysis effluent is interrogated with the broadband chirp and then undergoes free induction decay (FID). For the safety of the detection electronics and to minimize interference, a switch is used after the receiving horn. A low-noise amplifier amplifies the molecular signal. After frequency down-conversion, the FID is averaged and digitized by a real-time digitizer (Guzik ADC6131, 13 GHz analog bandwidth) with a 40 GSa/s sampling rate. Twenty 16 μs long FIDs were collected within each gas pulse, resulting in a nominal frequency resolution of 60 kHz. To reduce noise from the TWTA in the early part of the FID, time-domain signals were subjected to a Kaiser-Bessel windowing function with a shape parameter of 11.5, before taking the Fast Fourier Transform. These components are frequency referenced by a 100 MHz quartz oscillator driven by a 10 MHz Rb oscillator (Stanford Research Systems FS725).

Mass Spectrometer: After interrogation of the sample with microwaves, the jet-cooled gas pulse continues downstream where the coldest part of the gas pulse is sampled through a 2 mm diameter skimmer, located 35 cm from the pulsed valve, into the ionization region of the TOF mass spectrometer. To generate the soft ionization VUV source, with an energy of 10.5 eV (118 nm), the 3rd harmonic (355 nm) of a Nd:YAG laser (Continuum YG661-20(680)) is focused through a 31 cm long gas cell filled with a gas mixture of Xe (10 torr)/Ar (100 torr), where frequency tripling takes place.[32] Using off-axis propagation, the quartz entrance lens and MgF_2 lens at the end of the VUV cell spatially filter and focus the 118 nm beam relative to the 355 nm pump beam. The laser pulse is triggered by a digital delay generator (Berkeley Nucleonics model 577) controlled by the AWG. Components of the reaction mixture are ionized by VUV radiation via a one-photon process in the extraction region between the repeller plate (+3000 V) and the draw-out grid (+2750 V), and the cations are focused by ion optics (einzel lens, +1700 V) onto the surface of a microchannel plate (MCP) detector (Jordan TOF Products, Inc., C0701). The resulting current is amplified by a fast amplifier (Stanford Research Systems SR445) and displayed on a 3.5 GHz, 40 GSa/s oscilloscope (Tektronix DPO 7354C).

Rotational Spectral Fitting: Rotational Spectra of 3-PN and 4-PN with ^{14}N hfs, and internal rotation of 3-PN were fit to Watson's-S reduced Hamiltonian using SPFIT/SPCAT as part of the CALPGM suite.[33] In the present work also, we employed the SPFIT/SPCAT to predict rotational transitions for the 2,4-PDN molecules using Watson's-S reduced Hamiltonian within the 8-18 GHz region based on the fits obtained

by the Wisconsin group in the mmW region.[15] As the rotational characterization of 2,4-PDN was carried out in the mmW region, we did not have an accurate nuclear quadrupolar coupling constant due to ^{14}N in the 8-18 GHz region. Due to the weak signal and very few observed rotational transitions in our experiment, we could not fit hfs components of the observed tZ-2,4-PDN. In this article, the carbon atom labeling follows its position starting from the nitrile group of both the 3-PN and the 2,4-PDN systems, for example, C(5) position of 3-PN refers to the C atom in the terminal methyl group.

B. Computational Methods

Geometries of various C_5H_7N, C_5H_6N, and C_5H_5N species as well as their dissociation fragments were optimized at the B3LYP/6-311G(d,p) level of theory[34,35] and their vibrational frequencies were computed using the same method to evaluate zero-point vibrational energy corrections (ZPE). Single-point energies of the optimized structures were refined using the explicitly-correlated coupled clusters CCSD(T)-F12 approach[36,37] with Dunning's correlation-consistent cc-pVTZ-f12 basis set.[38,39] The CCSD(T)-F12/cc-pVTZ-f12//B3LYP/6-311G(d,p) + ZPE(B3LYP/6-311G(d,p)) relative energies are expected to be typically accurate within 4 kJ mol^{-1} or better.[40] The Gaussian 09[41] and MOLPRO 2010[39] program packages were used for the *ab initio* calculations.

Geometry optimizations and harmonic vibrational frequency calculations of all isomers and conformers of 2,4-PDN using Gaussian 09 suite of programs,[41] were also performed at the DFT B3LYP-GD3BJ level of theory with the Def2TZVP basis set,[42,43] which corrects for the dispersive interactions and calculates reliable relative energies for medium-sized molecules.[4,44,45]

III. Results

A. VUV Photoionization Mass Spectra

The temperature of the pyrolysis microreactor was scanned from around room temperature (290 K) up to 1220 K, with the best product signal optimized at 1100 K. Pyrolysis reaction intermediates were observed in the VUV photoionization TOF mass spectrum at 900 K and above. We show mass spectra recorded at 960, 1040 and 1100 K in **Figure 1**.

Based on the mass spectra, we recorded broadband microwave spectra of 3-PN and its pyrolysis products over the 8-18 GHz range, averaging 1 million FIDs at 290 K and 1040 K and 3 million FIDs at 1100 K to get a better signal-to-noise ratio for small rotational transitions that showed up only at pyrolytic temperatures. The CP-FTMW spectrum of the pyrolysis reaction at 1100 K is shown in **Figure 2**. The mass spectrum assisted the analysis of our broadband rotational spectrum.

Photoionization of the reaction intermediates was carried out using 118 nm VUV pulses generated by tripling in a Xe/Ar mixture. VUV single-photon ionization is a soft ionization technique with an energy of 10.5 eV. Hence, all the peaks that show up in **Figure 1** correspond to chemical species with ionization potentials less than 10.5 eV, while those with IPs greater than this value are not detectable. This tends to discriminate against detection of small molecules, which often have IPs that exceed 10.5 eV.

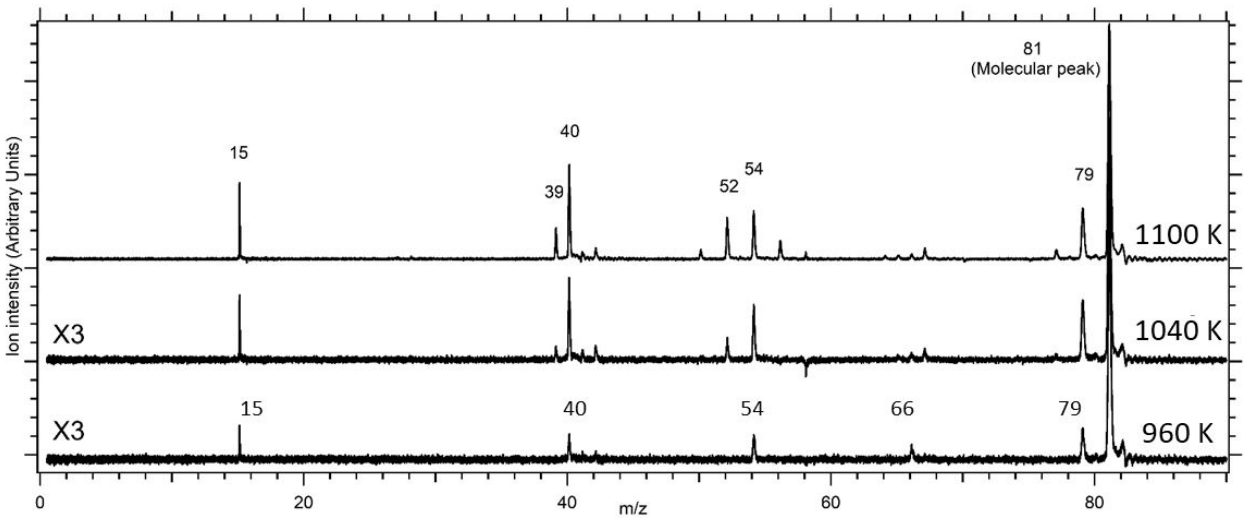

Figure 1: VUV photoionization TOF mass spectra of the flash pyrolysis intermediates products of 3-pentenenitrile at 960, 1040, and 1100 K. The spectra are normalized to the 3-PN molecular signal.

Our precursor 3-PN, with a mass of 81 Da, has molecular formula C_5H_7N, and is labeled as the molecular peak in **Figure 1**. At 290 K, the 118 nm TOF mass spectrum of 3-PN contains only the parent mass, confirming that no fragmentation occurs during the photoionization process. At a pyrolysis source temperature of 960 K, product peaks at 15, 40, 54, 66, and 79 Da begin to appear. Since these products appear at the lowest pyrolysis temperatures, they are formed early in the pyrolysis pathway, and are likely candidates as primary pyrolysis products. This is confirmed directly for the 15 and 66 Da peaks, whose masses sum to 81 Da, the mass of 3-PN starting material. This pathway, then, involves methyl loss from C_5H_7N to form C_4H_4N.

The peak at 79 Da arises from loss of 2 amu, equivalent to two H atoms or an intact H_2 molecule. Both H and H_2 have IPs above 10.5 eV and thus cannot be observed in our experiment. There is only the smallest hint of a peak at 80 Da due to loss of a single H-atom to form a free radical C_5H_6N product, suggesting that, if it is formed, it readily decays by loss of a second H-atom prior to interrogation. The 79 Da peak could correspond to multiple neutral structures with chemical formula C_5H_5N, including the heteroaromatic pyridine, or conjugated chain nitriles like 2,4-PDN. Four isomers of 2,4-PDN exist that are E/Z about the C(2)=C(3) double bond and *cis/trans* about the C(3)-C(4) single bond.

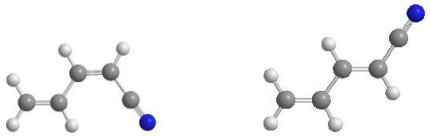

Trans-Z-2,4-PDN *Trans-E-2,4-PDN*

Other higher-energy, and therefore less likely, candidates for a 79 amu product are 3-pentynenitrile (75 kJ/mol), 3,4-pentadienenitrile (70 kJ/mol), 2,3-pentadienenitrile (57 kJ/mol), and 2-cyano-1,3-butadiene (*gauche*: 10 kJ/mol, *anti*: 23 kJ/mol), all calculated at the dispersion-corrected B3LYP-GD3BJ/Def2TZVP level of theory.

One of the peaks appearing in the TOFMS at all temperatures in **Figure 1** is at mass 40, which could correspond to allene ($H_2C=C=CH_2$), cyanomethyl radical ($H_2\dot{C}CN$), or propyne ($HC\equiv CCH_3$), all of which have ionization potentials below 10.5 eV. If this product is a primary product of 3-PN decomposition, its partner peak would be at 41 Da, with molecular formula C_3H_5 or CH_3CN. While the C_3H_5 product would

be observed in our 118 nm TOFMS, CH_3CN would not. Since we do not observe this m/z 41 product experimentally, we surmise that C_3H_5 is not formed or undergoes further reaction as it is formed. Similar arguments hold for the peak at 54 amu, due to C_4H_6, which is either 1,3- or 1,2-butadiene. Its product partner would appear at 27 Da, the mass of HCN. Since HCN has an IP (13.6 eV) well above 10.5 eV, it is not observed in the 118 nm TOFMS.

The most prominent secondary products appear in the TOF mass spectrum at 39 and 52 Da, which grow in relative to the primary products at higher temperatures. The 39 Da peak is likely due to the resonance-stabilized propargyl radical ($HC{\equiv}C\dot{C}H_2$) while the 52 Da peak (C_4H_4) has the molecular formula of vinylacetylene. Such secondary products most likely arise from subsequent unimolecular decomposition of the primary products. We will consider pathways to their formation in the discussion section.

In addition to these prominent secondary products, several small peaks appear at higher temperatures. These could arise from primary radicals attacking the precursor or reacting with other primary products. The fact that we observe no products with masses larger than 81 Da argues against addition reactions of primary radicals with the precursor. The small size of these additional peaks is consistent with a bimolecular step involving two low-concentration intermediates, which will not be considered further.

B. Broadband Microwave Spectra

At these pyrolysis source temperatures, several new transitions were detected in the 8-18 GHz CP-FTMW spectrum (**Figure 2**) that were not present at room temperature. When the pyrolysis source was heated, the MW transitions due to 3-PN were rotationally warmer and their intensity was stronger than at room temperature due to indirect warming of the sample compartment.[4] Hence, to identify transitions from pyrolysis reaction intermediates and products, we first assigned and removed lines due to the precursor molecule. We then carefully searched for rotational transitions corresponding to vibrationally excited states, which would appear as vibrational satellites. To identify such transitions in *syn* 3-PN, we performed anharmonic frequency calculations using the dispersion corrected DFT B3LYP/Def2TZVP. Using the coupling terms (α_{Ai}, $\alpha_{Bi,}$ α_{Ci}) between the rotational moments of inertia along the three axes (A, B, and C) and the corresponding vibrational modes, shifts from the zero-point rotational constants were predicted (See **Supplementary Information and Table S1**). No transitions due to vibrationally excited states could be identified, probably because the lowest modes of vibration in *syn* 3-PN have frequencies greater than 100 cm^{-1}.

Next, we looked for rotational transitions due to ^{13}C isotopologues using calculated rotational constants obtained at the B3LYP-GD3BJ/Def2TZVP level of theory. We identified all five ^{13}C isotopologues for the precursor *syn* 3-PN, which are labeled $^{13}C(1)$, $^{13}C(2)$, $^{13}C(3)$, $^{13}C(4)$, and $^{13}C(5)$ where the C atom numbering in parentheses starts from the nitrile group of *syn* 3-PN. The ^{14}N nuclear quadrupolar coupling and methyl internal rotation were not considered in the isotopologue fitting process as there were very few lines that displayed clear hyperfine splittings due to weak signal intensities. Best-fit rotational constants for all the ^{13}C isotopologues (using the SPFIT fitting program[33] and PIFORM from PROSPE website[46]) are listed in **Table 1,** and the experimental line lists are presented in **Table S2**. The SPFIT/SPCAT input files are available in the **Supplementary Information**. We could not find the ^{15}N isotopologue of *syn* 3-PN.

We did not attempt to look for the vibrational satellites and isotopologues of the minor conformer of 3-PN, *eclipsed* 3-PN, as the microwave transition intensities due to this conformer are about 15% of those due to the *syn* isomer, and therefore would not be detected at the present signal-to-noise ratio. After filtering out the precursor transitions within the MW spectrum, and armed with knowledge of the molecular formulae of the species present in the expansion from the VUV TOFMS, the number of structures we needed to look for in the MW spectrum was reduced considerably.

Table 1 Best-Fit rotational parameters[33] of the ^{13}C isotopologues of *syn* 3-PN. The 1-σ standard error for each rotational constant is given in parentheses.

Rotational parameters	$^{13}C(1)$	$^{13}C(2)$	$^{13}C(3)$	$^{13}C(4)$	$^{13}C(5)$
A (MHz)	8161.52(21)	7998.32(35)	8064.010(16)	8149.6(21)	8124.42(17)
B (MHz)	1919.3310(15)	1934.2305(28)	1936.91120(13)	1929.356(16)	1888.2331(13)
C (MHz)	1583.6245(15)	1587.4046(27)	1591.81350(12)	1589.946(15)	1561.01630(99)
RMS (kHz)	7	12	1	68	23
Number of lines	6	6	5	6	4

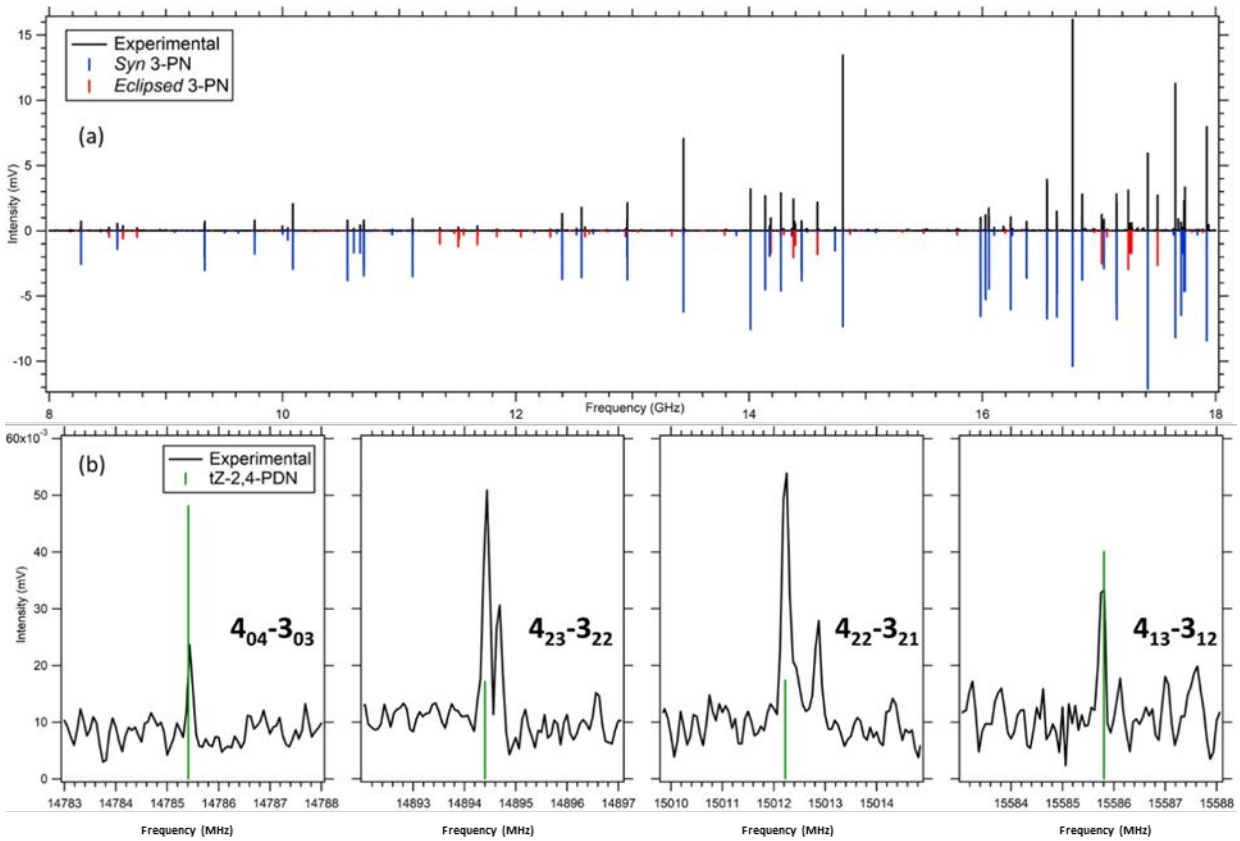

Figure 2: (a) Broadband microwave spectrum of the pyrolysis of *trans* 3-pentenenitrile with the pyrolysis source at 1100 K in the 8-18 GHz range. The experimental spectrum (black trace) is a 3 million average scan with argon backing gas. Using the known rotational constants for 3-pentenenitrile,[4] transitions due to the *syn* (blue trace) and the *anti* (red trace) structures of the precursor are shown. **(b)** Individual transitions of the pyrolysis product *trans*-Z-2,4-pentadienenitrile that were not present in the spectrum recorded with the pyrolysis source at 290 K. Predicted frequencies for the indicated rotational transitions of *trans*-Z-2,4-pentadienenitrile are shown in green, lying within the instrumental resolution of our experimental trace (black trace).

Our primary focus was identifying the structure of C_5H_5N (m/z=79). We carefully searched for transitions due to pyridine within the MW spectrum, but no evidence could be found. However, using the experimental rotational fit parameters for the pentadienenitrile isomers from the Wisconsin group[15] we were able to identify four transitions corresponding to tZ-2,4-PDN within our MW spectrum recorded at both 1100 K and 1040 K. All four observed transitions are *a*-type J=4↔3 transitions; specifically, 4_{04}-3_{03}, 4_{23}-3_{22}, 4_{22}-3_{21}, and 4_{13}-3_{12} (**Figure 2(b)**). Although the s-*trans*-E-2,4-pentadienenitrile (tE-2,4-PDN) is predicted by calculations to lie within 1 kJ mol^{-1} of tZ-2,4-PDN (**Table S3**), we could not confirm its presence in the MW spectrum, a puzzling result to which we will return in the discussion. Similarly, transitions due to the corresponding *cis* isomers of 2,4-PDN were also not observed experimentally. These *cis* isomers are calculated to have energies 15 kJ/mol higher than their *trans* counterparts (**Table S3**) and are thus not anticipated to be formed with significant population.

We also searched the MW spectrum for rotational transitions due to nitrile-containing molecules and radicals lighter than m/z=79. Of primary interest here was the C_4H_4N intermediate (66 amu) formed by loss of methyl (15 amu) from 3-PN (81 amu). Note that while the peak at 66 Da is observed at the lowest temperature in the VUV TOFMS (**Figure 1**), it loses intensity relative to other peaks at higher temperatures. Despite its large dipole moment as a nitrile, no microwave transitions due to C_4H_4N could be assigned. We surmise on the basis of both the mass spectrometric and microwave evidence that the 66 amu primary thermal decomposition product must itself decompose efficiently under the conditions of our experiment.

Small molecules such as HCN and CH_3CN that are not detected with 118 nm photoionization, also do not have rotational transitions within the 8-18 GHz range of our CP-FTMW spectrum due to their large rotational constants. While the $\dot{C}H_2CN$ radical (40 amu) has an IP (9.9 eV) low enough to make it detectable with 118 nm photoionization, its lowest frequency microwave transition is near 20 GHz, and therefore also just out-of-range of our detected microwave range.[47] Pyrolysis reaction products that are aliphatic unsaturated hydrocarbons (m/z=52 and 54) also could not be observed in the microwave spectrum due to their small dipole moments (μ< 0.5 D).

IV. Discussion

Calculations of the stationary points on the ground state C_mH_nN potential energy surfaces relevant to 3-PN thermal decomposition were performed at the CCSD(T)-F12/cc-pVTZ-F12//B3LYP/6-311G**+ZPE(B3LYP/6-311G**) level of theory to decipher our experimental observations. These results are summarized in **Figure 3**. In order to emphasize the different experimental observations that the calculations must predict, we highlight in green the primary products of mass 15, 40, 54, 66, and 79 in the 118 nm photoionization mass spectrum, those observed in both mass and microwave spectra in red, the mass 80 isomers and others predicted by the calculations as primary thermal decomposition products of 3-PN in blue, and the secondary products predicted by calculations and observed in the mass spectrum in tan.

A. Formation of *t*-Z-2,4-PDN (C_5H_5N, 79 amu)

The peak at 79 Da in the 118 nm TOFMS (**Figure 1**) was identified as tZ-2,4-PDN in the MW spectrum recorded at a pyrolysis source temperature of 1100 K (**Figure 2(b)**). As can be seen in **Figure 3(a)**, the pyrolysis reaction pathway to tZ-2,4-PDN starting from both the 3-PN conformers involves sequential loss of 2 H-atoms and not concerted H_2 elimination. These two H-atoms are lost from the C(2) and C(5) positions, leading to a net π-bond formation. Although initial H-atom loss from either C-atom position is possible, loss at C(2) (next to the nitrile group) is energetically favored over C(5) by about 30 kJ/mol, with a calculated bond dissociation energy of 337 kJ/mol (80.5 kcal/mol). The resonance stabilized radical (RSR) intermediate $CH_3CHCH\dot{C}HCN$ so formed has 5-center π-electron delocalization, whereas loss at the C(5) position produces the 3-center RSR $\cdot CH_2CHCHCH_2CN$. Of course, the reverse is true for the second H-atom loss, with overall energy barriers for formation of 2,4-PDN + 2H of 545-551 kJ/mol relative to the 3-PN precursor.

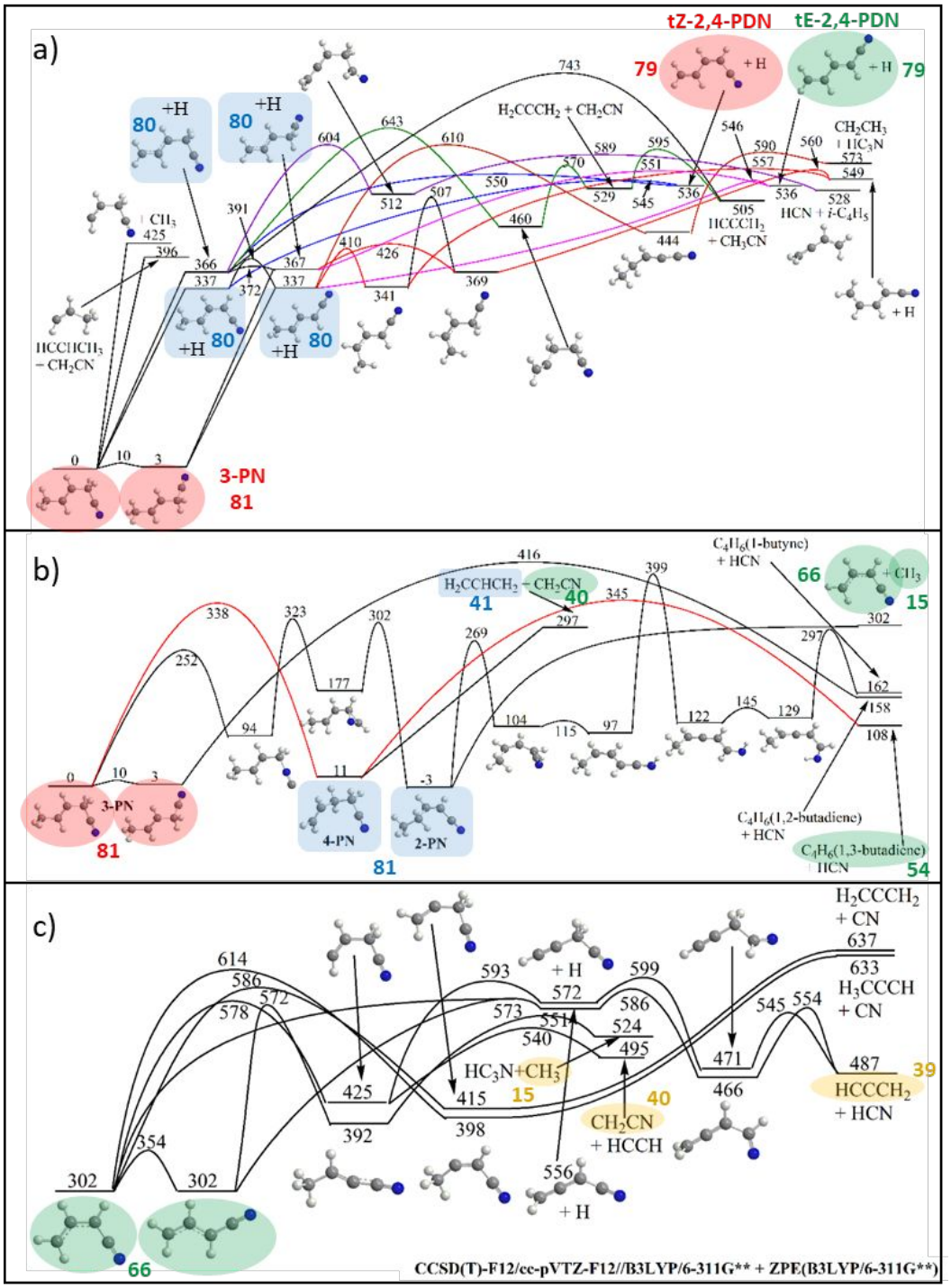

Figure 3: Potential energy surfaces for the thermal decomposition of 3-pentenenitrile. Pathways from 3-PN initiated by **(a)** bond breaking and **(b)** isomerization. **(c)** Secondary reactions arising from the 66 amu intermediate. The energies at the stationary points are given in kJ mol^{-1} relative to the most stable structure, *syn* 3-pentenenitrile. The structures shaded in red are those that are observed in both the 118 nm VUV photoionization mass spectrum (**Figure 1**) and the CP-FTMW spectrum (**Figure 2**), those shaded in green (tan) are primary (secondary) products that appear only in the mass spectrum (**Figure 1**), while those in blue were not detected by either means, but are identified by calculations as significant primary decomposition products of 3-PN. See text for further discussion.

In what follows, we refer to the 2,4-PDN product as a primary product in the sense that loss of the second H-atom is facile, with the 80 Da intermediate (shaded in blue) not observed. Not only is H-atom loss facile, but there are no weak C-C bonds in this intermediate, with all its population undergoing loss of a second H-atom to form 2,4-PDN.

The pathways, barrier heights, and final product energies for formation of the C_5H_5N isomer tE-2,4-PDN + 2H are very similar to those for tZ-2,4-PDN. As a result, it seems unlikely that formation of the tE isomer would be discriminated against significantly relative to the tZ isomer. Furthermore, the dipole moments of the two isomers are similar, arguing against significant differences in detection sensitivity in the microwave.[15] We thus do not have a firm explanation for not observing the tE-2,4-PDN isomer in the CP-FTMW spectrum and anticipate that with higher sensitivity, both isomers would be observed.

On the other hand, the inability to detect pyridine in the microwave spectrum, when combined with the computational evidence based on the potential energy surface in **Figure 3**, provides strong evidence that the mass 79 product contains no pyridine. Thus, unsaturated nitriles such as 3-PN may often prefer alternative thermal decomposition pathways to those involving ring closure.

B. Pathways initiated by isomerization

One of the interesting aspects of the pyrolysis of 3-PN is that it has both nitrile and vinyl functional groups in its structure, separated from one another so that they seemingly would act independently. However, in searching for pathways to masses 66, 15, 40, and 54 that could compete with the initial H-atom loss step, with its dissociation threshold of 337 kJ/mol, direct fragmentation from 3-PN was unable to account for our observations in a consistent way. As a result, we also explored pathways initiated by isomerization of 3-PN to its structural isomers 2-PN and 4-PN, which are shown in **Figure 3(b)**. Experimentally, we had dismissed isomerization from our early consideration because we had studied the microwave spectroscopy of 4-PN and searched for its presence in the broadband microwave spectrum of 3-PN pyrolysis to no avail. We also looked for 2-PN transitions based on the predictions of calculations of its rotational constants and saw no clear evidence for it.

Nevertheless, isomerization is almost certainly at play in the thermal decomposition of 3-PN. For instance, the loss of the terminal methyl group in 3-PN would account for the products of mass 15 and 66 observed in the VUV TOF mass spectrum. However, simple fragmentation of the C(4)-C(5) bond has a calculated BDE of 425 kJ/mol (**Figure 3(a)**), some 88 kJ/mol higher in energy than the H-atom loss channel. However, the lowest energy isomerization pathway from 3-PN to 2-PN involves a three-step process with rate-limiting barrier of 323 kJ/mol (**Figure 3(b)**). This pathway involves rearrangement of the terminal nitrile group to its isonitrile isomer followed by two H-atom transfer steps that produce 2-pentenenitrile (2-PN), with an energy just slightly below that of 3-PN. The 2-PN isomer has a terminal ethyl group with a much weaker C(4)-C(5) bond for methyl loss (305 kJ/mol) because it forms the 1-nitrile allyl (CH_2=CH-ĊH-CN) resonance-stabilized radical, the 66 Da intermediate with structure shown in green in **Figure 3**. While the ion signal at mass 15 is robust at all temperatures, the ion signal at 66 Da is not, indicating that the latter product decomposes further at higher temperatures. As a result, we were not able to detect this resonance-stabilized derivative of the allyl radical in the microwave spectrum.

In a similar fashion, there exists a single-step pathway for HCN loss from 3-PN (**Figure 3(b)**) to form mass 54 products that are prominent in the lowest temperature VUV photoionization TOF mass spectrum (**Figure 1**). However, it passes through a transition state 416 kJ/mol above *syn* 3-PN, and therefore will not compete with H-atom loss and CH_3 loss. Instead, we proposed the pathway shown in red in **Figure 2(b)** as the preferred pathway to loss of HCN, proceeding by isomerization through a transition state of 338 kJ/mol to form 4-PN, a slightly less stable pentenenitrile isomer. However, 4-PN can lose HCN via a single-step transition state of 345 kJ/mol, producing 1,3-butadiene (54 Da). This will occur in competition with breaking the central C(2)-C(3) bond of 4-PN to produce a pair of resonance-stabilized radicals, allyl radical (C_3H_5, 41 Da) and cyanomethyl (CH_2CN, 40 Da). The BDE for this step is just 286 kJ/mol (297 kJ/mol relative to 3-PN), and would account for the signal in the VUV TOFMS at mass 40. Furthermore, the allyl radical itself can readily expel an H-atom to form allene (not shown in **Figure 3**) with an established BDE of 232.8 kJ/mol.[48] This explains why the allyl product (mass 41) is not observed in the VUV spectrum.

C. Secondary Product formation

Figure 3(c) follows the decomposition of the *cis* and *trans* isomers of the 1-nitrile allyl radical (CH_2=CH-$\dot{C}$H-CN, 66 Da) from 2-PN dissociation, in order to help establish why this primary product never builds in concentration with temperature. Once again, isomerization by intramolecular H-atom transfer appears to play a role. *Cis* 1-nitrile allyl can undergo a 1,3-H-atom shift over a 276 kJ/mol barrier (578 relative to 3-PN) to form the original C_4H_4N isomer that would have been formed by breaking the C(4)-C(5) bond in 3-PN (**Figure 3(a)**). Subsequent fission of the weak central C-C bond (BDE=115 kJ/mol) leads immediately to HCCH + $\dot{C}H_2$-CN (40 Da, shaded tan). HCCH has an IP (11.40 eV), too high to observe with 118 nm photoionization, while $\dot{C}H_2$-CN would add a secondary product pathway to the signal at mass 40. In competition with this pathway is one that leads to CH_3 + HC_3N. The methyl product (also shaded tan) would add to the ion signal at 15 Da in the TOFMS, while HC_3N (mass 51) has an IP of 11.6 eV, and thus is not ionized by 118 nm light.

The series of VUV TOFMS in **Figure 1** also identify secondary products at masses 39 and 52 that are not formed at the lowest temperatures but grow in at higher pyrolysis source temperatures. The latter product is almost certainly vinylacetylene (H_2C=CH-C≡CH) while mass 39 is assigned to the propargyl radical ($\dot{C}H_2$-C≡CH). We have identified two secondary pathways to the propargyl radical. Thermal decomposition of the 1,3-butadiene primary product has been explored in detail by Chambreau et al.[49] As in 3-PN, 1,3-butadiene undergoes isomerization by two successive intramolecular H-atom transfers over barriers of about 312 kJ/mol to form 1,2-butadiene, which subsequently decomposes to CH_3 + $HCCCH_2$ (mass 39). Alternatively, as **Figure 3(c)** shows, the mass 66 primary product can undergo a two-step process of H-atom loss from C(3) and addition to the nitrile carbon to form HCN + $\dot{C}H_2$-C≡CH. This seems a less likely option under our experimental conditions, as it involves a bimolecular step. Finally, we have not been able to identify a clear pathway to vinylacetylene (mass 52). Loss of two H-atoms from 1,3-butadiene is not significant relative to methyl loss. H-atom abstraction from 1,3-butadiene is a plausible alternative, but the mass 53 intermediate that would be formed is not observed.

V. Conclusions

The flash pyrolysis of the *trans* isomer of 3-pentenenitrile forms a rich variety of products due to both molecular and radical-forming pathways. The complementary experimental evidence provided by broadband microwave spectroscopy and 118 nm photoionization mass spectra enabled mass-correlated microwave spectra to be recorded.[24] When combined with a detailed computational investigation, we were able to account for all the observed primary products**.**

We are able to eliminate certain plausible pathways as energetically prohibitive relative to the loss of two H-atoms from 3-PN to form mass 79 products. The lowest energy thresholds involves H-atom loss at C(2) (337 kJ/mol) or C(5) (366 kJ/mol) leading to one of four isomeric C_5H_6N products that efficiently lose a second H-atom to form one of the isomeric forms of 2,4-pentadienenitrile (79 amu). We have detected the *trans*-Z isomer in the broadband microwave spectrum by matching with line positions from the authentic samples studied by the Wisconsin group.[15] Despite being energetically close to the spectroscopically observed *trans*-Z isomer of pentadienenitrile, we could not confirm the existence of the *trans*-E isomer in our microwave spectrum. Perhaps a different reaction initiating method (discharge or photolysis) can be employed to observe and study the relative populations of these two 2,4-pentadienenitrile isomers. No pyridine was detected under our experimental conditions.

The other primary products identified in the VUV TOFMS can only be accounted for following isomerization of 3-PN to either 2-PN followed by methyl loss, or 4-PN followed by either HCN loss or C(2)-C(3) bond dissociation to form two resonance stabilized products. Thus, the close energetic proximity between H-atom loss and H-atom transfer pathways leading to isomerization, produces a number of interesting primary products in the thermal decomposition of 3-PN, and is likely to be a signature of larger

molecules with more than one site of unsaturation. In order to see this more directly, it would be worthwhile and interesting to compare these results with analogous studies of 4-PN and 2-PN pyrolysis. Finally, after a complete PES analysis for the pyrolysis of 3-PN, we see that the secondary products (tan shaded) in **Figure 3** grow in only at higher pyrolysis temperatures, whereas the primary products (green shaded and tZ-2,4-PDN) occur throughout the range of pyrolysis temperatures, hence strengthening our claim.

The present results contribute to an understanding of astrochemical processing of nitriles in at least two ways. First, star-forming regions often have temperatures sufficiently high to thermally process nitriles,[50,51] especially ones that incorporate more than one functional group, as in 3-PN. Pathways that incorporate the nitrile functional group into a more complex organic framework, such as an aromatic ring, are particularly relevant for understanding how heteroaromatics are formed, a subject of intense interest in astrobiology.[13] Indeed, due to its recognized relevance to astrochemistry/astrobiology, various reaction pathways to the mass 79 isomers, 2,4-PDN and pyridine have been studied previously.

Second, in planetary atmospheres such as Titan, UV photoexcitation of 3-PN would lead to photochemical processing occurring either in one or more excited electronic states or after internal conversion to the ground electronic state. Once on the ground electronic surface, hot 3-PN would react as it does under pyrolysis conditions. As a result, the present work focuses attention on one aspect of the photochemistry and can help distinguish excited state from ground state processes in subsequent photochemical studies that contain contributions from both. Furthermore, once a C_5H_5N isomer such as 2,4-PDN is formed, it too can undergo photochemical excitation followed by internal conversion, providing the energy to photoisomerize on the C_5H_5N PES that includes pyridine, as predicted by Lin et al.[14]

Acknowledgments

We thank Robert J. McMahon from the University of Wisconsin-Madison for providing us with their line list and fitted rotational constants for several pentadienenitrile isomers and conformers prior to publication. PM thanks Dr. Brian M. Hays for useful discussions regarding microwave spectroscopy and the astrochemistry of nitrile compounds. PM and TSZ gratefully acknowledge support for this work from the Department of Energy Basic Energy Sciences Gas Phase Chemical Physics Program under grant DE-FG02-96ER14656. TSZ acknowledges support from the U.S. DOE, Office of Science, Office of Basic Energy Sciences during manuscript preparation at Sandia. Sandia National Laboratories is a multi-mission laboratory managed and operated by National Technology and Engineering Solutions of Sandia, LLC., a wholly owned subsidiary of Honeywell International, Inc., for the U.S. DOE National Nuclear Security Administration under contract DE-NA0003525.

References

1 B. A. McGuire, *Astrophys. J., Suppl. Ser.*, 2018, **239**, 17.

2 B. A. McGuire, A. M. Burkhardt, S. Kalenskii, C. N. Shingledecker, A. J. Remijan, E. Herbst and M. C. McCarthy, *Science*, 2018, **359**, 202.

3 F. Raulin, C. Brassé, O. Poch and P. Coll, *Chem. Soc. Rev.*, 2012, **41**, 5380.

4 P. Mishra, S. M. Fritz, B. M. Hays, D. N. Mehta-Hurt, K. M. Jawad and T. S. Zwier, *Phys. Chem. Chem. Phys.*, 2019, **21**, 23651.

5 M. Morisson, C. Szopa, N. Carrasco, A. Buch and T. Gautier, *Icarus*, 2016, **277**, 442.

6 M. McGuigan, J. H. Waite, H. Imanaka and R. D. Sacks, *J. Chromatogr. A*, 2006, **1132**, 280.

7 C. Sagan, W. R. Thompson and B. N. Khare, *Acc. Chem. Res.*, 1992, **25**, 286.

8 R. Moreno, E. Silla, I. Tunon and A. Arnau, *Astrophys. J.*, 1994, **437**, 532.

9 S. B. Morales, C. J. Bennett, S. D. Le Picard, A. Canosa, I. R. Sims, B. J. Sun, P. H. Chen, A. H. H. Chang, V. V. Kislov, A. M. Mebel, X. Gu, F. Zhang, P. Maksyutenko and R. I. Kaiser, *Astrophys. J.,* 2011, **742**, 26.

10 B. J. Sun, C. H. Huang, S. Y. Chen, S. H. Chen, R. I. Kaiser and A. H. H. Chang, *J. Phys. Chem. A*, 2014, **118**, 7715.

11 A. Jamal and A. M. Mebel, *J. Phys. Chem. A*, 2013, **117**, 741.

12 S. M. Kougias, S. N. Knezz, A. N. Owen, R. A. Sanchez, G. E. Hyland, D. J. Lee, A. R. Patel, B. J. Esselman, R. C. Woods and R. J. McMahon, *J. Org. Chem.*, 2020, **85**, 5787.

13 N. Kitadai and S. Maruyama, *Geosci. Front.*, 2018, **9**, 1117.

14 M. F. Lin, Y. A. Dyakov, C. M. Tseng, A. M. Mebel, S. H. Lin, Y. T. Lee and C. K. Ni, *J. Chem. Phys.*, 2005, **123**, 054309.

15 P. M. Dorman, V. L. Orr, M. A. Zdanovskaia, S. M. Kougias, B. J. Esselman, R. C. Woods, R. J. McMahon, Manuscript in preparation.

16 G. G. Brown, B. C. Dian, K. O. Douglass, S. M. Geyer, S. T. Shipman and B. H. Pate, *Rev. Sci. Instrum.*, 2008, **79**, 053103.

17 G. B. Park and R. W. Field, *J. Chem. Phys.*, 2016, **144**, 200901.

18 K. Prozument, G. Barratt Park, R. G. Shaver, A. K. Vasiliou, J. M. Oldham, D. E. David, J. S. Muenter, J. F. Stanton, A. G. Suits, G. Barney Ellison and R. W. Field, *Phys. Chem. Chem. Phys.*, 2014, **16**, 15739.

19 C. Abeysekera, L. N. Zack, G. B. Park, B. Joalland, J. M. Oldham, K. Prozument, N. M. Ariyasingha, I. R. Sims, R. W. Field and A. G. Suits, *J. Chem. Phys.*, 2014, **141**, 214203.

20 K. Prozument, Y. V. Suleimanov, B. Buesser, J. M. Oldham, W. H. Green, A. G. Suits and R. W. Field, *J. Phys. Chem. Lett.*, 2014, **5**, 3641.

21 B. C. Dian, G. G. Brown, K. O. Douglass and B. H. Pate, *Science*, 2008, **320**, 924.

22 N. M. Kidwell, V. Vaquero-Vara, T. K. Ormond, G. T. Buckingham, D. Zhang, D. N. Mehta-Hurt, L. McCaslin, M. R. Nimlos, J. W. Daily, B. C. Dian, J. F. Stanton, G. B. Ellison and T. S. Zwier, *J. Phys. Chem. Lett.*, 2014, **5**, 2201.

23 C. H. Townes and A. L. Schawlow, *Microwave Spectroscopy*, Dover Publications, New York, 1955.

24 S. M. Fritz, B. M. Hays, A. O. Hernandez-Castillo, C. Abeysekera and T. S. Zwier, *Rev. Sci. Instrum.*, 2018, **89**, 093101.

25 C. Abeysekera, A. O. Hernandez-Castillo, J. F. Stanton and T. S. Zwier, *J. Phys. Chem. A*, 2018, **122**, 6879.

26 P. Chen, S. D. Colson, W. A. Chupka and J. A. Berson, *J. Phys. Chem.*, 1986, **90**, 2319.

27 C. Karunatilaka, A. J. Shirar, G. L. Storck, K. M. Hotopp, E. B. Biddle, R. Crawley and B. C. Dian, *J. Phys. Chem. Lett.*, 2010, **1**, 1547.

28 D. P. Zaleski and K. Prozument, *Chem. Phys. Lett.*, 2017, **680**, 101.

29 J. M. Hudzik and J. W. Bozzelli, *J. Phys. Chem. A*, 2010, **114**, 7984.

30 J. M. Simmie, K. P. Somers, K. Yasunaga and H. J. Curran, *Int. J. Chem. Kinet.*, 2013, **45**, 531.

31 K. N. Urness, Q. Guan, T. P. Troy, M. Ahmed, J. W. Daily, G. B. Ellison and J. M. Simmie, *J. Phys. Chem. A*, 2015, **119**, 9962.

32 J. Yang, X. Bin Wang, X. P. Xing and L. S. Wang, *J. Chem. Phys.*, 2008, **128**, 201102.

33 H. M. Pickett, *J. Mol. Spectrosc.*, 1991, **148**, 371.

34 A. D. Becke, *J. Chem. Phys.*, 1993, **98**, 5648.

35 C. Lee, W. Yang and R. G. Parr, *Phys. Rev. B*, 1988, **37**, 785.

36 G. Knizia, T. B. Adler and H. J. Werner, *J. Chem. Phys.*, 2009, **130**, 054104.

37 T. B. Adler, G. Knizia and H. J. Werner, *J. Chem. Phys.*, 2007, **127**, 221106.

38 T. H. Dunning, *J. Chem. Phys.*, 1989, **90**, 1007.

39 H.-J. Werner, P. J. Knowles, R. Lindh, F. R. Manby, M. Schütz, P. Celani, T. Korona, G. Rauhut, R. D. Amos, A. Bernhardsson, et al., MOLPRO, Version 2010.1, A Package of Ab Initio Programs., University of Cardiff: Cardiff: UK, 2010.

40 J. Zhang and E. F. Valeev, *J. Chem. Theory Comput.*, 2012, **8**, 3175.

41 D. J. Frisch, M. J. Trucks, G. W. Schlegel, H. B. Scuseria, G. E. Robb, M. A. Cheeseman, J. R. Scalmani, G. Barone, V. Mennucci, B. Petersson, G. A. Nakatsuji, H. Caricato, M. Li, X. Hratchian, H. P. Izmaylov, A. F. Bloino, J. Zheng and G. Sonnenb, GAUSSIAN 09, Revision A. 1, Gaussian, Inc., Wallingford CT, **2009**.

42 S. Grimme, J. Antony, S. Ehrlich and H. Krieg, *J. Chem. Phys.* 2010, **132**, 154104.

43 S. Grimme, S. Ehrlich and L. Goerigk, *J. Comput. Chem.*, 2011, **32**, 1456.

44 P. Mishra, D. M. Hewett and T. S. Zwier, *J. Chem. Phys.*, 2018, **148**, 184304.

45 S. M. Fritz, P. Mishra and T. S. Zwier, *J. Chem. Phys.*, 2019, **151**, 041104.

46 PROSPE website: http://www.ifpan.edu.pl/Bkisiel/prospe.htm.

47 H. Ozeki, T. Hirao, S. Saito and S. Yamamoto, *Astrophys. J.*, 2004, **617**, 680.

48 B. S. Narendrapurapu, A. C. Simmonett, H. F. Schaefer, J. A. Miller and S. J. Klippenstein, *J. Phys. Chem. A*, 2011, **115**, 14209.

49 S. D. Chambreau, J. Lemieux, L. Wang and J. Zhang, *J. Phys. Chem. A*, 2005, **109**, 2190.

50 A. Coletta, F. Fontani, V. M. Rivilla, C. Mininni, L. Colzi, Sánchez-Monge and M. T. Beltrán, *Astron. Astrophys.*, 2020, **641**, A54.

51 R. Choudhury, P. Schilke, G. Stéphan, E. Bergin, T. Möller, A. Schmiedeke and A. Zernickel, *Astron. Astrophys.*, 2015, **575**, A68.